International Journal of Micro Air Vehicles

Original research article

International Journal of Micro Air Vehicles
Volume 17: 1–15

DOI: 10.1177/17568293251350056
journals.sagepub.com/home/mav
Sage

Impact of surface roughness on quasi-steady in-ground effect for hover-capable aerial vehicles

Cheng G Kou[1,2], James R Stoll[1] and Kam K Leang[1,2]

Abstract

Ground effect (GE) behavior occurs when a hover-capable multirotor aerial vehicle, such as a quadcopter, flies within close proximity to the ground and the vehicle experiences an increase in thrust despite constant power being applied to the propellers. Current GE models assume that the ground plane is flat and smooth. This paper investigates the influence of aerodynamically-rough surfaces on GE behavior for standard two-blade propellers under quasi-steady hover conditions. First, a nondimensional model is proposed that incorporates the aerodynamic roughness and zero-plane displacement height of a rough surface with GE parameters previously found in the literature. Second, a GE model that accounts for surface roughness is described. Third, physical experiments are conducted to quantify the aerodynamic properties of controlled rough surfaces and the GE strength through observations of in-ground effect (IGE) and out-of-ground effect (OGE) thrusts produced by commercially available propellers. The results show that aerodynamically rougher surfaces corresponded to higher IGE thrust. Fourth, statistical analysis of the results supported the accuracy of the proposed model, where the average root-mean-squared error is 0.90% with an average maximum error of 2.39% over all test scenarios. Finally, nondimensional analysis confirmed that when similarity conditions are met, the proposed model follows theoretical projections. These findings can be exploited for vehicle motion control, navigation, and design.

Keywords

In-ground effect, aerodynamic roughness, multirotor aerial vehicles

Received: 7 April 2024; accepted: 30 May 2025

Introduction

Hover-capable aerial vehicles that use propellers to generate lift are versatile and ubiquitous. For example, the Boeing H-47 Chinook rotorcraft is often used for transportation of military personnel and equipment, while smaller personal quadcopter uncrewed aerial vehicles (UAVs) are being used for photography, disaster management, agriculture, and remote sensing.[1–4] More recently, rotorcraft UAVs have been developed for autonomous environmental monitoring applications including chemical-leak identification, mapping, and localization.[5–10]

One of the main benefits of the rotorcraft design is its ability to hover, loiter, and slowly fly near the ground. However, as the propellers come close to the ground, increased thrust is observed, despite constant power being applied.[11–13] Stated another way, because of the increase in thrust, less power is required to maintain constant height while operating within the in-groud effect (IGE) zone. The natural phenomenon that occurs when the propellers are within "close" proximity to the ground is commonly known as *ground effect* (GE). The GE occurs due to the rotors' wake interacting with the disturbing entity.[14–17] Understanding GE behavior can be leveraged to improve rotorcraft design and motion control.[18,19] For example, previous ground effect modeling and experiments have been used to design control systems that compensate for IGE, substantially enhancing the

[1]Department of Mechanical Engineering, University of Utah, Salt Lake City, Utah, United States
[2]Robotics Center, University of Utah, Salt Lake City, Utah, United States

Corresponding author:
Kam K Leang, Department of Mechanical Engineering and Robotics Center, University of Utah, Salt Lake City, Utah, USA.
Email: kam.k.leang@utah.edu

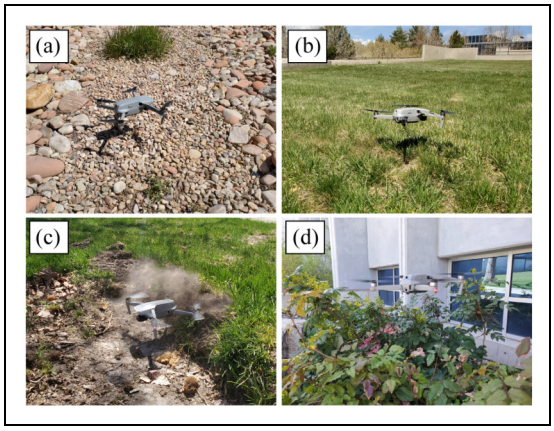

Figure 1. Quadcopter UAVs hovering in-ground effect over different terrain: (a) bed of rocks, (b) field of grass, (c) patch of dirt, and (d) plant with branches and leaves.

vehicle's take-off, landing, and near-ground flight performance.[18,20–23]

There are three main considerations when studying ground effect for a rotorcraft: (1) the rotor-blade geometry, (2) the nature of the fluid, and (3) the characteristics of the ground. This paper focuses on the latter, studying the impact of different ground surfaces, specifically their aerodynamic properties on GE. Currently, studies[13,16] that describe the impact of surface conditions on the ground effect on rotorcraft UAVs are limited. The main contribution herein is to bridge the existing knowledge gap.

Figure 1 shows examples of a quadcopter UAV hovering over different terrain within the IGE region. In Figure 1(a), the UAV hovering over a solid bed of rocks will experience GE at a different strength compared to hovering over grass (Figure 1(b)) or loose dirt (Figure 1(c)). Furthermore, hovering over dense grass will result in GE different from hovering over a bush (Figure 1(d)). Both are relatively elastic compared to rocks or soil. Previous works[13,16] have observed that different surfaces incur GE at different magnitudes, but no systematic study of the effect of surface roughness was performed. Therefore, the current understanding and application are confined to IGE on solid flat surfaces. Existing models are also unable to capture the impact of rough surfaces. Herein, the main contribution is to bridge the knowledge gap by performing experiments and developing a model that relates the IGE thrust ratio to surface roughness.

Although it has been mentioned in the literature,[13,16,24–27] the impact of different surfaces on the performance of a propeller IGE is not well understood. Some studies have briefly touched on this topic,[24,26,27] while others study the effects of partial ground and ceiling surfaces on propeller performance, showing how finite-size obstacles influence the thrust and power characteristics.[28] It has been suggested in He[24] that influences from a surface are due to the surface stiffness

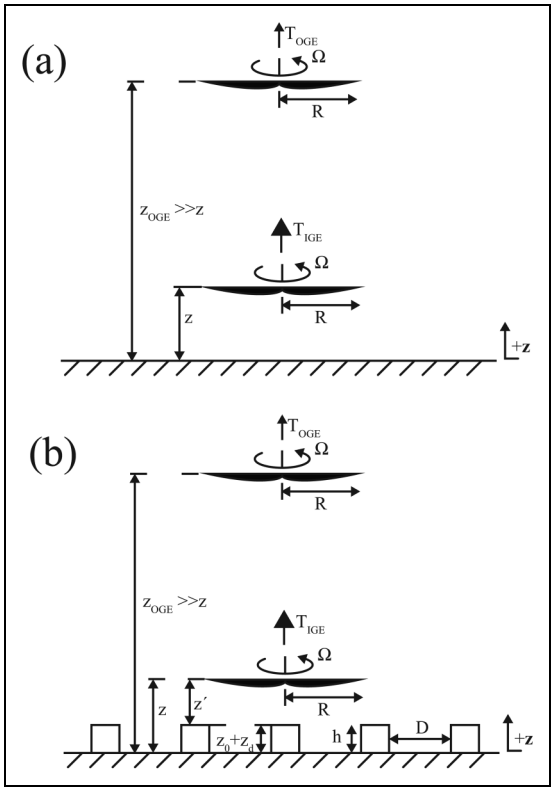

Figure 2. UAV propeller above a surface where ground effect is observed: (a) hovering IGE at height z and OGE at height zv_{OGE} over a smooth flat surface and (b) hovering IGE and OGE over a surface with roughness elements (RE) conceptualized as repeating blocks.

and aerodynamic roughness. In more general terms, the ground effect is determined by surface material properties and aerodynamic interactions with surface geometry. The focus of this work is the latter of the two, and the former is left as future work.

This work considers the two configurations shown in Figure 2, where the propellers are positioned above a surface on which GE is observed. Figure 2(a) shows two scenarios: a propeller hovering over a flat smooth surface (1) out-of-ground effect (OGE) and (2) IGE. Figure 2(b) shows the same situation, but the surface has roughness elements conceptualized as simple repeating blocks.

The main contributions of this work are: (1) an experimental characterization of the ground effect over surfaces with different roughness values, (2) an empirical IGE model that incorporates surface roughness based on non-dimensional analysis, and (3) the validation of the model through physical experiments.

Nomenclature

The following nomenclature is used in this paper:

A_f: frontal silhouette area of a single roughness element, m^2
A_p: plan area of all roughness elements, m^2
A_t: total area covered by roughness elements, m^2
C_{l_α}: 2D lift-curve slope, rad^{-1}
C_T: coefficient of thrust
D: distance between roughness elements, m
d: minimum tip-to-tip distance between propellers, m
h: roughness element height, m
K_G: in-ground effect thrust ratio
k: von Karman constant
k_Π: number of independent variables in a physical relationship
N_b: number of blades in a propeller[12]
P: power applied to a rotor, W
P_{atm}: atmospheric pressure, Pa
P_t: stagnation pressure, Pa
P_s: static pressure, Pa
p: number of governing independent dimensions in a physical relationship
R: propeller radius, m
Re: Reynolds number
T: thrust force, N
T_{IGE}: in-ground effect thrust, N
T_K: temperature, K
T_{OGE}: out-of-ground effect thrust, N
u: wind speed, m/s
u_*: shear velocity, m/s
V: rotorcraft velocity, m/s
v_i: induced velocity, m/s
z: height above the ground plane, m
z_d: zero plane displacement height, m
z_0: aerodynamic roughness length, m
γ: propeller pitch, m
δ_v: viscous sublayer height, m
θ_0: blade collective pitch angle, rad
λ_f: frontal area aspect ratio
λ_p: plan area aspect ratio
μ_a: advance ratio
μ: fluid dynamic viscosity, kg/m-s
ρ: fluid density, kg/m^3
σ: rotor solidity
Ω: rotor angular velocity, rad/s

Ground effect and aerodynamic roughness

Quasi-steady ground effect for two-blade propeller over flat smooth surfaces

The most fundamental study on ground effect focuses on a two-blade rotor in hover over a solid flat surface. In this quasi-steady state, ground effect is more evident than in other flight modes, such as forward flight.[11,29–31] In 1955, Cheeseman and Bennett[11] proposed a model to estimate the ground effect ratio, which has been used extensively to compensate for ground effect.[20–23,32] The model is derived analytically from the method of images and is confirmed to be reasonably accurate using empirical helicopter thrust data. Using thrust data, the ground effect ratio was calculated based on the height of the vehicle above the ground, z, and the radius of the propeller R. The ratio between the IGE and OGE thrust is given by

$$K_G = \frac{T_{IGE}}{T_{OGE}} = \frac{1}{1 - \dfrac{R^2}{16z^2}}, \quad \text{for, } z/\mathrm{R} > 0.5. \tag{1}$$

Note that in equation (1), $z/R \leq 0.5$ would be impractical since the helicopter fuselage would create an obstruction.

Another widely popular GE model was proposed by Leishman,[12] Eberhart,[16] Bernard et al.,[32] Hayden,[33] Pulla,[34] and Light,[35]

$$K_G = \frac{1}{0.9926 + 0.0379(2R/z)^2}. \tag{2}$$

This model has been noted to over predict the amount of IGE thrust.[12] Similar to equation (1), Hayden's relationship contains heights that result in singularities.

In an attempt to characterize a more universal expression, an exponential model was developed by He et al.,[18] He,[36] and He and Leang,[37] given by

$$K_G = C_a e^{-C_b z/R} + 1, \tag{3}$$

where C_a and C_b are coefficients determined by blade geometry. In a quick glance, the He et al., model lacks singularities due to the height where the GE thrust is finite, such as when the height $z = 0$. This model is chosen in this work because it has been shown to capture the GE behavior with good accuracy and it has been effectively used for GE compensation in flight control.[18]

In equation (3), coefficients C_a and C_b are functions of a propeller's geometry,[18,37] where C_a is derived from blade element theory and is expressed as

$$C_a = \frac{\sqrt{192C_{l_\alpha}\sigma\theta_0 + 9(C_{l_\alpha}\sigma)^2} - 3C_{l_\alpha}\sigma}{32\theta_0 + 3C_{l_\alpha}\sigma - \sqrt{192C_{l_\alpha}\sigma\theta_0 + 9(C_{l_\alpha}\sigma)^2}}, \tag{4}$$

and C_b is empirically found to be

$$C_b = 0.92\sigma + 1.23, \tag{5}$$

where C_{l_α} is the 2D lift-curve slope, σ is the propeller solidity, and θ_0 is the collective pitch angle. Moving forward, the He et al., model will be developed to incorporate the impact of aerodynamic surface roughness.

Aerodynamic surface roughness

The aerodynamic surface roughness is the height at which wind speed over a surface theoretically becomes zero due

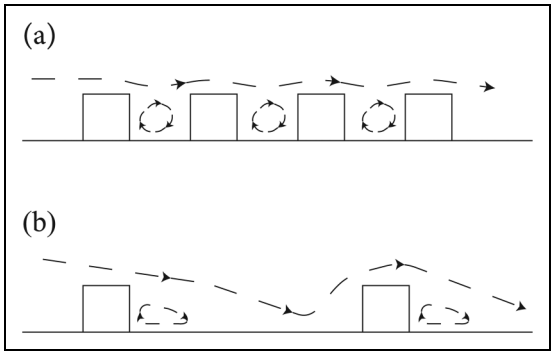

Figure 3. Example of (a) *d*-type and (b) *k*-type roughness.

to the shear stress or drag force over said surface. Often, it is accompanied by a zero-plane displacement height, which is manifested due to the density of roughness elements (RE) causing a skimming effect in the airflow.[38,39] Aerodynamic roughness is widely used in the meteorological community to describe the aerodynamics of complex geometries and terrain features in a succinct way.[40–47] In statically-neutral conditions, the relationship between wind speed and the ground's aerodynamic properties is given by

$$\frac{\overline{u}(z)}{u_*} = \frac{1}{\kappa}\ln\left(\frac{z - z_d}{z_0}\right), \tag{6}$$

where $\overline{u}(z)$ is the mean wind speed at height z above the ground plane, u_* is the shear velocity or friction velocity, which is a representation of the shear stress over a given surface in units of speed, κ is the von Karman constant usually taken to be $\kappa \in [0.35, 0.4]$, z_0 is the aerodynamic roughness length parameter, and z_d is the zero-plane displacement height.[38]

Although the aerodynamic roughness can be quickly calculated using wind speed measurements, there have been many attempts to characterize the length in terms of more easily observable geometric parameters, however, currently, all expressions for roughness and displacement height are purely empirical and rely heavily on RE of roughly the same size and shape.[40,41,44,45,48,49]

While equation (6) is mainly used for wind speed profiles over large terrain, the same velocity profile has been observed on smaller scales. Nikuradse,[50] and later Gul and Ganapathisubramani,[51] observed similar logarithmic velocity profiles in fluid pipe flow experiments. Roughness was artificially created by gluing sand grains to the inside of the pipes. Perry et al.[52] expanded the understanding of velocity profiles over rough surfaces by introducing the concepts of *d-type* and *k-type* roughness. Examples are shown in Figure 3, where *d*-type roughness (Figure 3(a)) involves RE packed tightly together and results in the skimming effect mentioned earlier. The *k*-type roughness (Figure 3(b)) takes place when the RE have ample spacing between themselves so that the eddies formed are shed with the main flow.

Table 1. Key variables used in nondimensional analysis for a two-blade propeller in IGE hover over a rough surface.

Repeating variable	Symbol	Unit	
Radius	R	cm	
Induced Velocity	v_i	m/s	
Fluid density	ρ	kg/m^3	
Non-repeating variable	Symbol	Unit	Π group
IGE thrust	T_{IGE}	N	$\Pi_1 = T_{IGE}/\rho R^2 v_i^2$
Height above surface	z	m	$\Pi_2 = z/R$
Aerodynamic roughness	z_0	mm	$\Pi_3 = z_0/R$
Zero-plane displacement	z_d	mm	$\Pi_4 = z_d/R$
Collective rotor pitch	θ	rad	$\Pi_5 = \theta_0$
Chord length	c	cm	$\Pi_6 = c/R$
2D lift-curve slope	C_{l_α}	rad^{-1}	$\Pi_7 = C_{l_\alpha}$
Fluid viscosity	μ	Kg/ms	$\Pi_8 = \mu/\rho v_i R$

In both types of roughness, extrapolation of the logarithmic flow profile shows a theoretical zero velocity above the ground plane correlating to an aerodynamic roughness and zero-plane displacement height. However, in *d*-type roughness, the zero-plane displacement height would play a larger role in determining the flow profile, whereas in *k*-type roughness the displacement height is minimal in effect.

Nondimensional model

The Buckingham Π Theorem is often used to formulate a nondimensional relationship for any physical phenomenon by considering key variables relating to geometric characteristics, material properties, and external effects, such as velocity or forces.[53] For GE thrust analysis in the presence of surface roughness, key variables can be found by considering properties of the surface, rotor, and air. The key (repeating and non-repeating) variables for the nondimensional analysis are summarized in Table 1.

The IGE thrust, T_{IGE}, is chosen as the variable of interest. The first variable important to the IGE thrust is the distance, z, between the rotor and ground planes. Because of their wide application for describing surface roughness on multiple scales and in various compositions, key variables relating to the surface are the aerodynamic roughness, z_0, and zero-plane displacement height, z_d. The most important rotor variable is the radius, R. Other key rotor variables have previously been identified in He et al.,[18] He,[36] and He and Leang[37] and include the collective pitch θ_0, chord length c, and 2D lift-curve slope C_{l_α}. In other notable works, a propeller pitch γ, in units of distance, is used in lieu of the closely related collective pitch.[28,54–56] The last group of variables relate to the air itself, including the induced velocity on the air by the rotor v_i, the density of the air ρ, and dynamic viscosity μ.

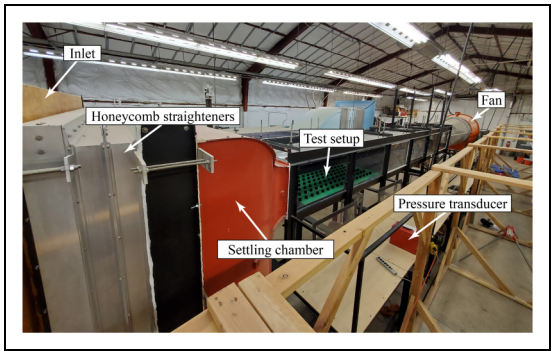

Figure 4. Exterior view of the open-circuit wind tunnel setup.

The OGE thrust value can be rewritten as a function of the rotor radius, induced velocity, and fluid density using momentum theory,[12]

$$T_{OGE} = 2\rho\pi R^2 v_i^2. \tag{7}$$

These three variables can conveniently be used as repeating variables to nondimensionalize the other variables. The resulting Π groups are summarized in Table 1. From them, a relationship for the IGE thrust ratio can be expressed as

$$\frac{T_{IGE}}{T_{OGE}} = \frac{T_{IGE}}{\rho R^2 v_i^2} = \phi\left(\frac{z}{R}, \frac{z_0}{R}, \frac{z_d}{R}, \theta_0, \frac{c}{R}, C_{l_a}, \frac{\rho v_i R}{\mu}\right), \tag{8}$$

where each term from left to right represents Π groups 1-8 sequentially and ϕ is the function relating Π group 1 to the others. It is of note that Π group 8 has been inverted here to depict the rotor Reynolds number in a more traditional form.

Ground effect model for surface roughness

Aerodynamic roughness, z_0, and zero-plane displacement height, z_d, are surface roughness parameters that quantify the aerodynamic interactions between a rough ground and the fluid flow over it. These two parameters represent the height of the momentum sink in the fluid flow above a surface.[57,58] Similar to wind flowing over a terrain, it is hypothesized that these heights also act as a momentum sink to the rotor wake that interfaces with the ground, and thus, these height parameters alter the effective distance between the propeller and ground. As shown in Figure 2(b), a new effective height above ground, z', can be calculated after knowing the roughness and displacement height values. Extending this to the GE thrust ratio model (equation (3)), the proposed model that incorporates surface roughness is

$$K_G = \frac{T(z)}{T_\infty} = C_a e^{-C_b z'/R} + 1, \tag{9}$$

where the coefficients C_a and C_b are the same ones used in equation (3) and z' is defined as

$$z' = z - z_0 - z_d. \tag{10}$$

The proposed model assumes a generally homogeneous distribution of roughness and is applicable to quasi-steady hover for a two-blade propeller IGE.

Comparing the model, equations (9) and (10), to the nondimensional model in equation (8), the Π groups relating to height and the aerodynamics of a surface, z/R, z_0/R, and z_d/R, are present. Furthermore, Π groups 5-7, describing the geometry of the propeller, can be found in the equations defining coefficients C_a (equation (4)) and C_b (equation (5)). It is noted that Π_6 is represented as rotor solidity σ. This parameter is the ratio of the blade area over the disk area. Without loss of generality, a propeller can be thought of as having a rectangular shape, thus solidity is

$$\sigma = \frac{N_b c R}{\pi R^2} = \frac{N_b c}{\pi R}. \tag{11}$$

In this form, Π_6 is present. Finally, Π_8, the rotor Reynolds number, is missing from the proposed model; however, it has been shown that for small UAVs, the angular velocity of the propeller has no significant effect on the ground effect thrust ratio at speeds typical for flight.[15] Assuming those conditions are met, the rotor Reynolds number from the nondimensional model can be discounted in the proposed model without great consequence.

Experimental apparatuses

Two main experimental apparatuses were developed and used to observe and quantify GE of a two-blade propeller in quasi-steady hover over artificially-generated rough surfaces. First, the aerodynamic parameters of rough surfaces were measured in a wind tunnel. Second, the GE thrust produced by propellers of varying size over rough surfaces were measured.

Rough-surface elements

Rough surfaces were generated by mating RE composed of LEGO™ bricks, arrayed in a grid pattern, to a LEGO base plate. Individual blocks, representing the RE, had dimensions of roughly 32-mm length by 32-mm width by 38.4-mm height, excluding the height of the studs. The spacing, D, of adjacent blocks was varied to provide surfaces with reliably differing roughness values. Adjacent blocks were spaced 32, 64, 96, and 128-mm apart. A fifth surface covered only with LEGO base plates and no blocks was also tested. Finally, a flat concrete surface was used as a control surface.

Wind tunnel test facility and conditions

Surface roughness experiments were performed in an open circuit tunnel, as shown in Figure 4. A fan in the rear draws

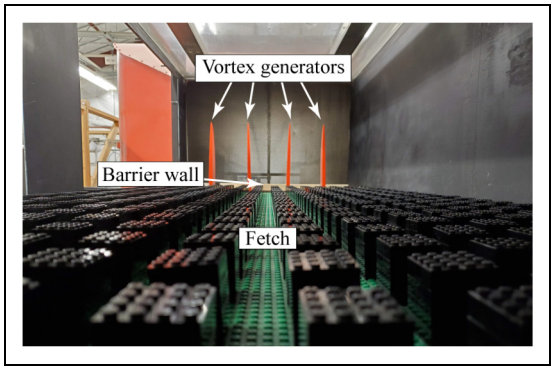

Figure 5. Experimental setup from inside the wind tunnel facing the inlet.

air into the inlet, then moves the air through the honeycomb straighteners and settling chamber for flow conditioning before flowing over the test setup. A pitot tube was used to capture the logarithmic wind-speed profile over each test surface by taking wind-speed measurements at varying heights above the RE.

To properly create the logarithmic wind-speed profile required to calculate the aerodynamic roughness of each surface, a fully developed turbulent flow that simulates an atmospheric boundary layer (ABL) is required.[53,59] The method Counihan[60] established was shown to create flow conditions similar to the ABL inside a wind tunnel with no major spanwise variation and his method was employed here. Figure 5 is a view of the interior setup; showing vortex generators and a barrier wall used to create artificial ABL conditions over the fetch of RE. Static conditions in the wind tunnel were neutral (*i.e.,* no buoyancy) and the lowest height probed was no less than 1.5 to 2 times the average height of the RE as stipulated by Macdonald et al.[41] and Wiernga.[47] A combination of a barrier and vortex generators (VG) were used to "trip" the airflow (see Figure 5). The vortex generators (VGs) take the shape of a quarter-elliptical wedge with an angle between 5 and 6 degrees. The height of the VGs can vary, but determines the approximate height of the modeled ABL.[60,61] Vortex generators were spaced 0.5 to 0.6 times the height of the generators from each other. The barrier wall was 1/8 the height of the VGs and placed no more than about 5/6 the height of the VGs in front of the VGs. The fetch required was at least 4 to 5 boundary-layer heights.

Details of test propellers

Six commercial-off-the-shelf (COTS) two-blade carbon fiber propellers of varying sizes were tested. The specifications for each propeller are found in Table 2, where each propeller has an associated reference number indicated by "ID No.". Size indicates the manufacturer's designated propeller size where the number preceding the "x" is the propeller diameter, the number after is the propeller pitch, both in units of *inches*, and "L" indicates a clockwise-rotating propeller. In Table 2, R denotes propeller radius, $\overline{c}$ is average cord length, θ_0 is collective pitch, and C_{l_α} is the 2D-lift curve slope. The 2D lift-curve slope C_{l_α} was calculated from GE thrust data collected over a smooth flat surface (curve-fit parameter) and using equation (4).

Table 2. Specifications for six propellers used during ground effect measurement experiments.

ID No.	Size	R (cm)	$\overline{c}$ (cm)	θ_0 (deg.)	C_{l_α} (N/(degree angle of attack))
16	16×5.4L	20.32	3.09	9.3	2.87
15	15×5L	19.05	2.89	10.2	3.43
14	14×4.8L	17.78	2.66	9.5	3.16
13	13×4.4L	16.51	2.46	9.3	3.29
11	11×3.7L	13.97	2.27	9.3	4.07
9	9×3L	11.43	1.73	9.3	8.12

Ground effect measurement Process

The GE phenomenon can be observed by comparing IGE and near-OGE (NOGE) thrust values. To measure propeller thrust values, a custom ground effect test stand, shown in Figure 6, was designed and built which automatically raises and lowers an attached propeller to specified heights before activating the propeller, taking measurements, and remotely reporting subsequent average thrust values to a nearby computer for post-processing and analysis. Propeller thrust values were measured using a lever-type mechanism where the propeller is on one end and a load cell resides on the other as shown in Figure 6.

Similar to Figure 2(b), a propeller actuated over a test surface made up of a block array, is taken from heights within the GE region to NOGE heights. A relatively smooth and flat concrete surface below the propeller, was used as a control surface (see Figure 2(a)). To capture the GE profile, thrust values from a propeller under test were measured at incremental heights over each test surface. The ground effect test stand was set to bring a propeller to specified heights depending on the radius of the propeller under test to ensure both IGE and NOGE thrust values were measured. Previous studies have shown that for propellers of radius R, the IGE region occurs at heights, z, roughly less than 2 times that of the propeller's radius, hence $z/R \lesssim 2$.[12,24,25] In this work, the maximum heights chosen were roughly 3 times that of the propeller radius, while the minimum heights chosen were approximately 2 times that of an single RE to minimize the impact of individual RE.

Following conclusions drawn from He and Leang,[15] and Bernard et al.,[62] the angular velocity rather than applied power was kept constant. This was accomplished by specifying pulse-width modulation signals to the motor

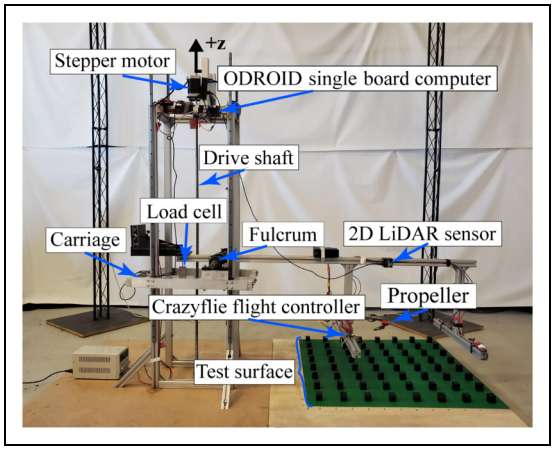

Figure 6. Experimental setup for ground effect measurement along the z-axis.

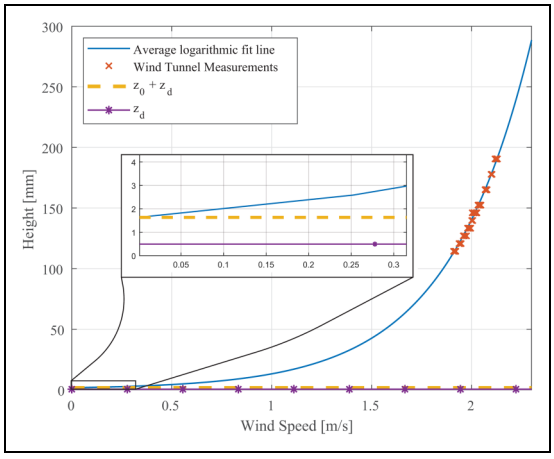

Figure 7. An example of wind tunnel measurements fitted to equation (6) for the surface with RE spaced 128-mm apart.

electronic speed controller. It is of note, that while traditional ground effect experiments either focus on maintaining constant thrust or power, it has been shown experimentally, that for small rotorcraft such as small UAVs, applying constant angular velocity, rather than power, can result in accurate IGE thrust ratio measurements.[15,24,62]

Results, analysis, and discussion

Wind tunnel results

The results acquired in the wind tunnel include the wind-speed measurements, aerodynamic roughness, and displacement height. The wind speed measurements at various heights over each test surface were fitted to equation (6) to estimate the aerodynamic roughness and displacement height values. An example using the measurements from the surface with RE spaced 128 mm apart is plotted in Figure 7. The full summary of values calculated for each test surface is given in Table 3, as well as the estimated values using empirical models found in Grimmond and Oke,[40] Lettau[44] and Kutzbach.[49] While estimating z_0 and z_d, the impact of studs on the blocks and LEGO plates were considered negligible due to their small size relative to the blocks themselves. On the LEGO plate surface without block elements, the studs were used to determine the estimates. The flat cement control surface, while not measured in wind tunnel experiments, is assumed to be aerodynamically smooth.

Table 3. Comparison between measured values for aerodynamic roughness z_0 and zero-plane displacement height z_d and estimations found using formulas derived empirically by kutzbach (*Ku*),[49] lettau (*Le*),[44] and counihan (*Co*)[40] for each test surface. NE denotes no elements.

D (mm)	z_0 (mm)	$z_{0,Ku}$ (mm)	$z_{0,Le}$ (mm)	z_d (mm)	$z_{d,Ku}$ (mm)	$z_{d,Co}$ (mm)
32	4.18	8.02	5.76	12.45	25.69	11.91
64	3.68	3.21	2.56	4.19	20.30	4.30
96	2.12	1.67	1.44	1.79	17.18	1.64
128	1.14	1.01	0.92	0.49	15.10	0.41
NE	0.37	0.38	0.10	0.00	1.11	0.57

Estimates using methods from Grimmond and Oke,[40] Lettau[44] and Kutzbach.[49] are based on either the plan area index, the ratio of RE plan area to the total area covered, or the frontal area index, the ratio of RE facial area normal to the direction of airflow to the total area covered. As shown by Grimmond and Oke,[40] there exists a sizeable margin of reasonable roughness parameters for any given plan area or frontal area index. Comparing the measured roughness parameters to the calculated estimates, it can be seen that they are within the order of magnitude from one another. Given that the scale is in millimeters and combining it with,[40] the values measured from experiments are fair.

It is worth noting that the use of LEGO blocks creates a rather homogeneous surface pattern resulting in a uniform roughness. Real world surface roughness will have localized variations depending on their surface composition. This study seeks to limit such factors so that the effect of surface roughness can be studied in a more direct manner.

Ground effect results

The ground-effect profile can be easily visualized as rotor thrust ratios at different heights. Figure 8 shows the results of the measured GE thrust ratio at the sampled heights over the surfaces with RE spaced 32 and 96 mm apart compared to the surfaces without roughness elements and without the studded plates for propeller 16. It illustrates a common theme: generally, as the roughness $(z_0 + z_d)$ increases, the thrust ratio increases.

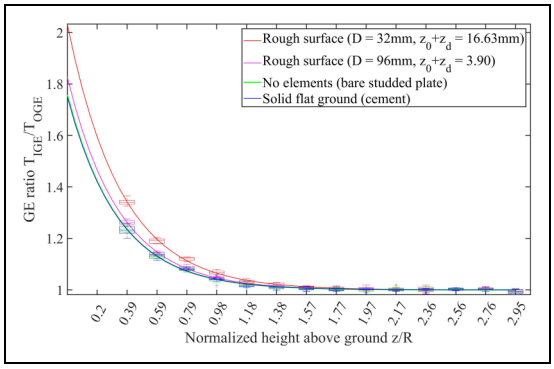

Figure 8. Measured IGE thrust ratios across the array of sampled heights over surfaces of varying roughness for propeller 16. Surfaces selected for display were limited for clarity.

The measured ground effect thrust ratios, across all surfaces, decrease exponentially as the height of the propeller from the surface increases. In fact, the underlying characteristic relationship between the thrust ratio and propeller height is exponential of the same form as the model in equation (3). Motivated by this observation, the following form is used to quantify the effect of surface roughness on the GE thrust ratio:

$$K_G = C_\alpha e^{-C_\beta z/R} + 1. \tag{12}$$

In model equation (3), the coefficients C_a and C_b are defined by the geometry of the propeller. For the model equation (12), the coefficients C_α and C_β physically represent the maximum GE increment and distribution of GE over height, respectively. These coefficients parameterize the exponential form of the model and can be empirically determined from measured data. For example, Figures 9 and 10 show the calculated C_α and C_β values, respectively, from measured ground effect thrust ratios for each propeller over each test surface.

Comparing the standard deviations of the GE coefficients between the different propellers, it is first concluded that propellers 9 and 11 have significant outliers not ideal for further analysis. This may be due to the lack of sensitivity of the instruments used in observing ground effect at the smaller scale. The analysis to validate the proposed model will focus on the results obtained from the larger propellers, namely propellers 13 to 16.

Statistical analysis and discussion

From Figures 9(a)-(d), it can be seen that surfaces with increased roughness generally correlate with higher maximum increases in ground effect, and as mentioned, the smaller the propeller, the less the trend is visible, as illustrated in Figures 9(e) and (f). This is especially apparent when data from each propeller is plotted on the same graph, as in Figure 11. Statistical analysis was performed between the datasets for each propeller to determine whether or not this observation is supported. Student's t-tests were used to compare the means of each dataset. Student's t-tests are an established method to determine whether the means of the test datasets were significantly different from the control or not.[63] A p-value is the probability of obtaining results equal to or more extreme than the observed data.[64] The calculated p-values between each test dataset and the control are presented in Table 4. Using a typical alpha-value of 0.05, it can be seen that there were significantly different means for datasets from rougher surfaces, and the results in Figures 9(a)-(d) confirm that the difference between the control and a rough surface is negative. Additionally, Table 4 shows that p-values generally decrease as the aerodynamic roughness of a surface increases. This translates to the probability that the average maximum increase in ground effect between the control and test surfaces were significantly different increases as roughness increases. The results of the t-test largely confirm that surfaces with higher roughness results in higher maximum increases to the ground effect observed.

The next question to answer is whether the proposed model can accurately predict the increase. Using the proposed model, equation (9), and the model for IGE thrust over a solid flat surface, equation (3), an expected increase in C_α due to a rough surface can be calculated for each dataset. Subtracting the predicted increase from each observation results in an adjusted dataset for each test surface which can be shown to be equivalent to the control surface.

T-tests were used to confirm whether or not the difference between the control and adjusted values are significant (Table 5). Rough surfaces with means previously shown to be significantly different than the control no longer support the same conclusion. Additionally, the p-values from the adjusted data no longer follow a decreasing trend with higher roughness. A single outlier correlates to propeller 15 over the surface with elements spaced 128-mm apart.

The proposed model's predicted C_α values can be compared graphically to the average measured C_α values (as shown in Figure 12). A linear regression of the data gives

$$y = 0.02 + 0.97x$$

with a R^2 value of 0.74.

According to the proposed model, the distribution of ground effect strength over height, encapsulated in coefficient C_β, should not change with roughness because the exponential term accounts for surface roughness using an adjusted height found in equation (10). The C_β values for each test surface is compared to the control C_b by calculating the associated p-values (Table 6). Using an alpha value of 0.05, results indicate that some of the measured mean C_β values were significantly different from that of the control. The p-values do not highlight any immediate trends connecting C_β to roughness or D/R. There are statistically different C_β means to the surfaces with blocks spaced 64- and

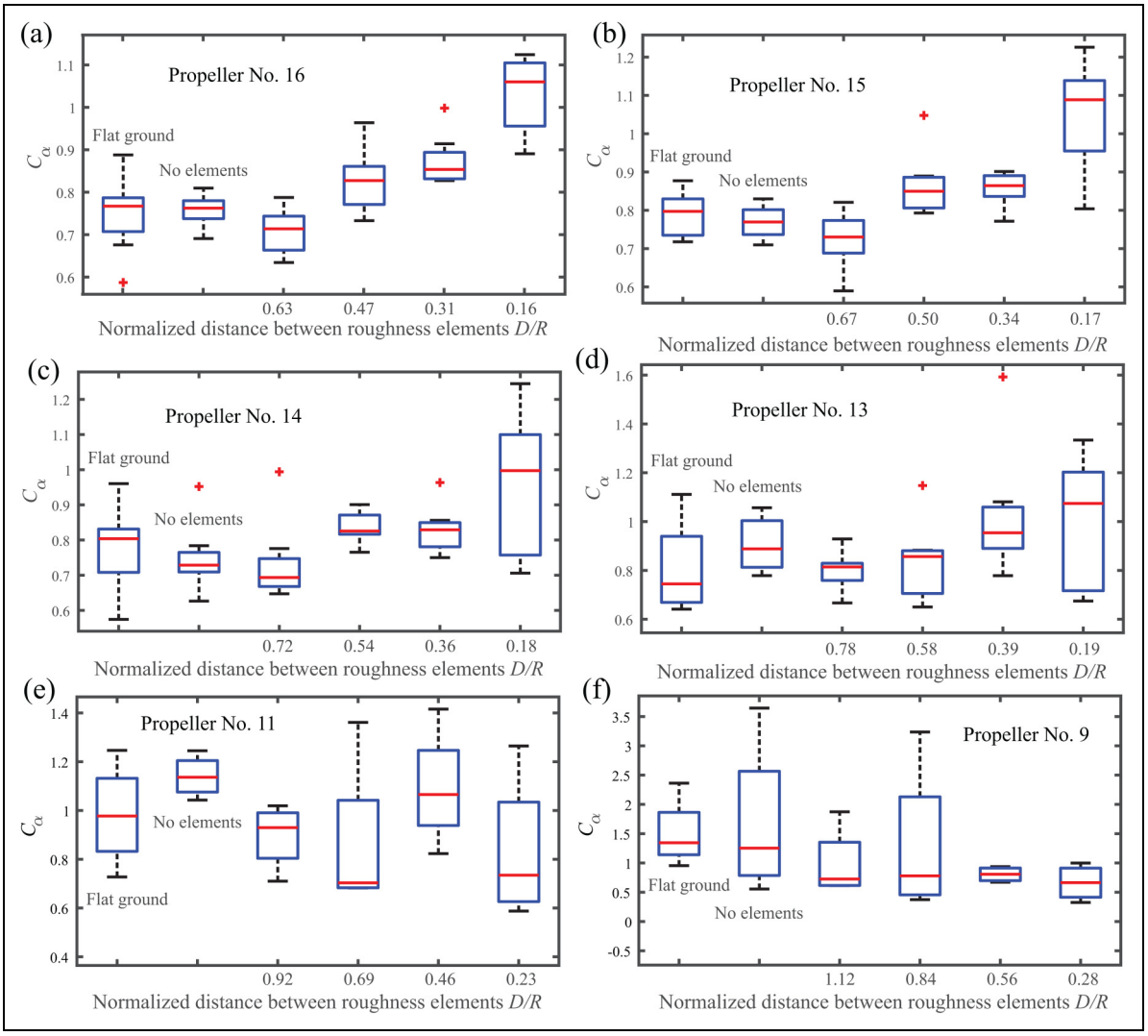

Figure 9. The calculated GE C_α coefficient from measured GE thrust ratios, through equation (12), for different propellers: (a) ID No. 16, (b) ID No. 15, (c) ID No. 14, (d) ID No. 13, (e) ID No. 11, and (f) ID No. 9.

128-mm apart, however, the other surfaces don't share that observation. The trend of statistically different means don't follow a consistent pattern of decreasing C_βs as D/R decreases. This could indicate there is more to the discrepancy than solely D/R, however, more research into the underlying causes of C_β is needed. The rest of this paper will focus on C_α, which provides more insights.

Predicted GE thrust ratios can be compared with the recorded data. The root-mean-squared error (RMSE) and maximum error can be calculated and used as a metric to evaluate the accuracy of the proposed model as a whole. The RMS and maximum errors for each propeller over each test surface are shown in Tables 7 and 8, respectively, and reported as a percentage of the mean measured data. The RMSE averaged over all figures is 0.90% and the average maximum error is 2.39%. The standard deviation averaged over all test datasets is 0.83%. The average RMSE is well below 2 standard deviations and the average max error is within 3 standard deviations. This indicates that the proposed model's predictions are within the natural noise of the observed GE. In general, the errors are quite low. The results strongly suggest that the proposed model can accurately predict the strength of ground effect over rough surfaces, despite observed statistically significant differences in the C_β and C_b coefficients.

Nondimensional analysis and discussion

The theory of models can be applied to further validate the proposed GE model. Let the physical model be propeller 16 in quasi-steady IGE hover over the surface with blocks spaced 32-mm apart and let the physical systems to be predicted be the propellers 13, 14, and 15, also in quasi-steady IGE hover over the same block array. The nondimensional

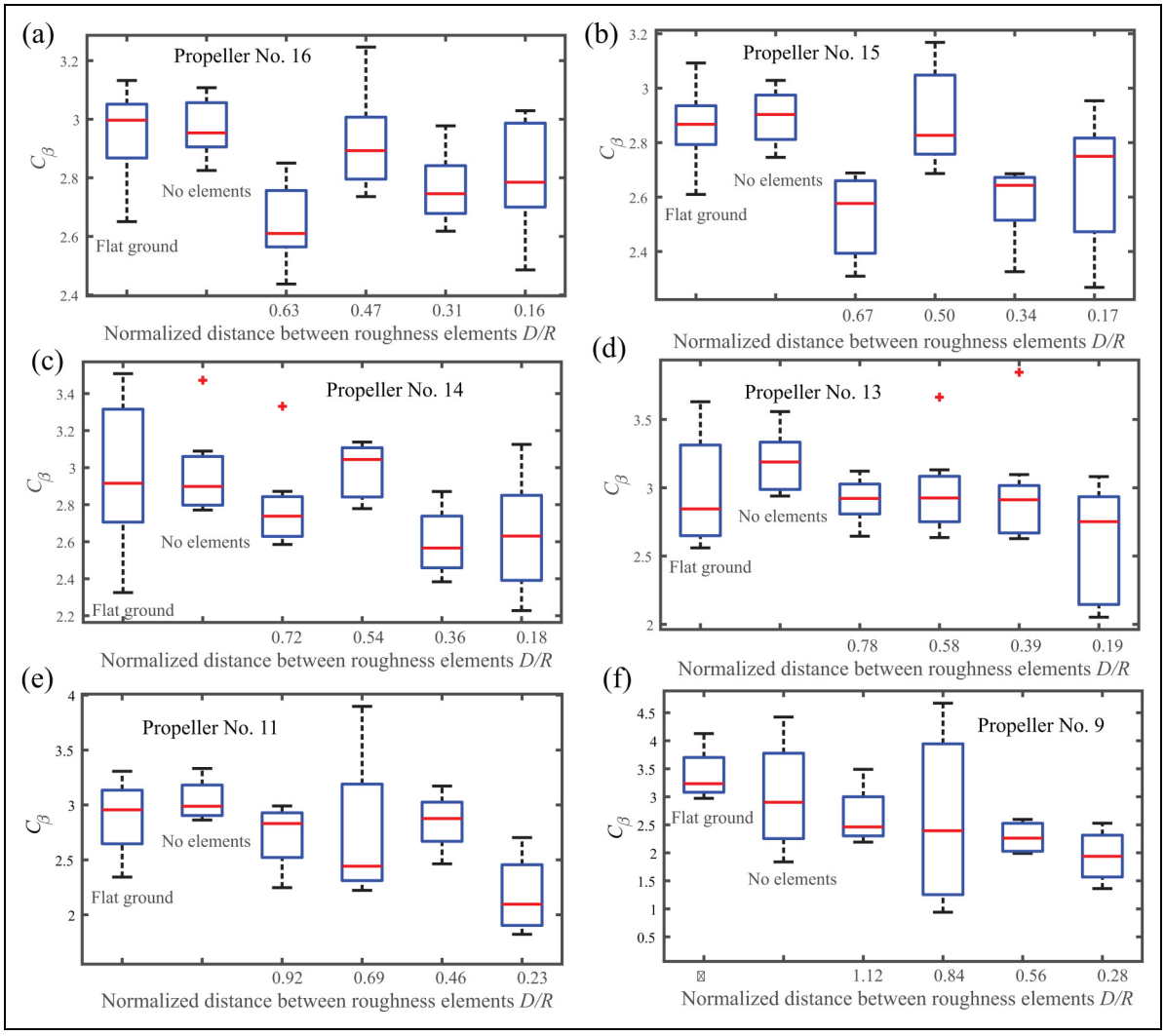

Figure 10. The calculated GE C_β coefficient from measured GE thrust ratios, through equation (12), for different propellers: (a) ID No. 16, (b) ID No. 15, (c) ID No. 14, (d) ID No. 13, (e) ID No. 11, and (f) ID No. 9.

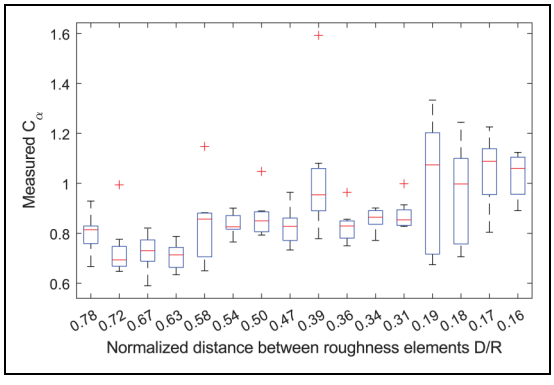

Figure 11. Combined measured GE C_α coefficients from propellers 16, 15, 14, and 13 plotted against D/R.

relationship governing both model and physical systems is captured in equation (8). Attempts to match the Π groups to meet similarity conditions quickly demonstrate that they cannot be met individually. A distorted model will be used instead, hence

$$\frac{T_{IGE}}{\rho R^2 v_i^2} \approx \phi'\left(\frac{z-(z_0+z_d)}{R},\ C_a,\ C_b\right). \tag{13}$$

Table 4. The p-values from the results of student t-tests comparing the average C_α values of the control to each test dataset.

	Distance between RE D.				
ID No.	NE	128 mm	96 mm	64 mm	32 mm
16	0.82	0.27	0.08	0.01	0.00
15	0.43	0.07	0.05	0.02	0.00
14	0.58	0.44	0.20	0.29	0.04
13	0.20	0.92	0.74	0.07	0.11

Table 5. The p-values of the student t-test comparing the control C_α values to that of the adjusted datasets based on the expected increase from equation (9).

	Distance between RE D.				
ID No.	NE	128 mm	96 mm	64 mm	32 mm
16	0.91	0.13	0.42	0.40	0.10
15	0.34	0.02	0.44	0.23	0.53
14	0.52	0.26	0.88	0.24	0.41
13	0.22	0.65	0.72	0.41	0.43

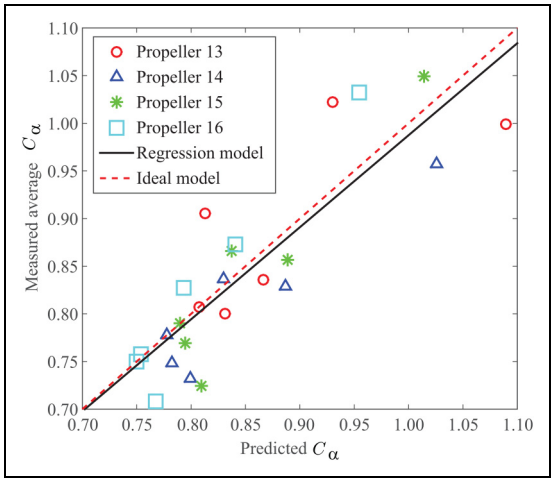

Figure 12. Regression analysis comparing the proposed model's predicted maximum increase in ground effect C_α to the measured averages of each surface for each propeller.

In the distorted model, a single composite dimensionless height term is used in lieu of the Π groups 2 through 4. Equations (4) and (5) show that coefficients C_a and C_b are functions of Π groups 5 through 7, thus C_a and C_b are used to represent blade geometry in the distorted model. Finally, assuming typical rotor speeds for a small UAV are used, the rotor Reynolds number can be excluded because inflow velocity and rotor angular velocity have a direct relationship to each other.[12]

To meet similarity conditions, the same range of dimensionless heights, per the distorted model, were used while conducting analysis for each of the models and system propellers. T-tests between measured model coefficients C_a and C_b and those of the physical systems, were conducted to show the differences were not significantly different. The resulting p-values from the t-tests are shown in Table 9.

The GE thrust ratios over a meaningful range of dimensionless heights were calculated using the proposed model, equation (9), for the model and physical systems under observation (Figure 13). Initial consideration of the datasets suggest model and physical system closely mirror each other as expected from the application of the theory of

Table 6. The p-values of the student's t-test comparing the average C_β values of the control to each test dataset.

	Distance between RE D.				
ID No.	NE	128 mm	96 mm	64 mm	32 mm
16	0.78	0.00	0.71	0.02	0.12
15	0.62	0.00	0.73	0.00	0.07
14	0.97	0.33	0.88	0.04	0.09
13	0.21	0.68	0.99	0.93	0.09

Table 7. The root-mean-squared error (RMSE) of thrust ratios calculated from the proposed model compared with the actual data measured over each dataset, as a percentage of the mean measured data.

	Distance between RE D.				
ID No.	NE	128 mm	96 mm	64 mm	32 mm
16	0.30	1.48	0.47	1.04	1.28
15	0.58	0.72	1.66	0.95	1.23
14	0.75	1.62	0.27	1.11	1.01
13	0.69	0.36	0.58	0.87	1.09

Table 8. The maximum thrust ratio errors from the proposed model compared to the actual data measured over each dataset, as a percentage of the mean measured data.

	Distance between RE D				
ID No.	NE	128 mm	96 mm	64 mm	32 mm
16	0.51	4.66	1.09	2.31	3.22
15	1.36	1.99	6.03	2.33	2.81
14	1.78	6.13	0.46	2.41	2.56
13	1.06	1.04	1.13	2.22	2.75

Table 9. The p-values of t-tests comparing the C_a and C_b coefficients between model (propeller 16) and physical systems (propellers 13, 14, and 15).

ID No.	C_a	C_b
13	0.42	0.88
14	0.60	0.94
15	0.30	0.25

models. More thorough analysis using T-tests, with an alpha value of 0.05, to compare the datasets at each dimensionless height between model and the physical systems indicates no significant differences. The only exception being the results encapsulated in the box shown in Figure 13 (a), which correlates to propeller 15. This may be ascribed to its C_a and C_b coefficients. Per Table 9, propeller 15 has the highest probability in having a significant difference between model and physical system values.

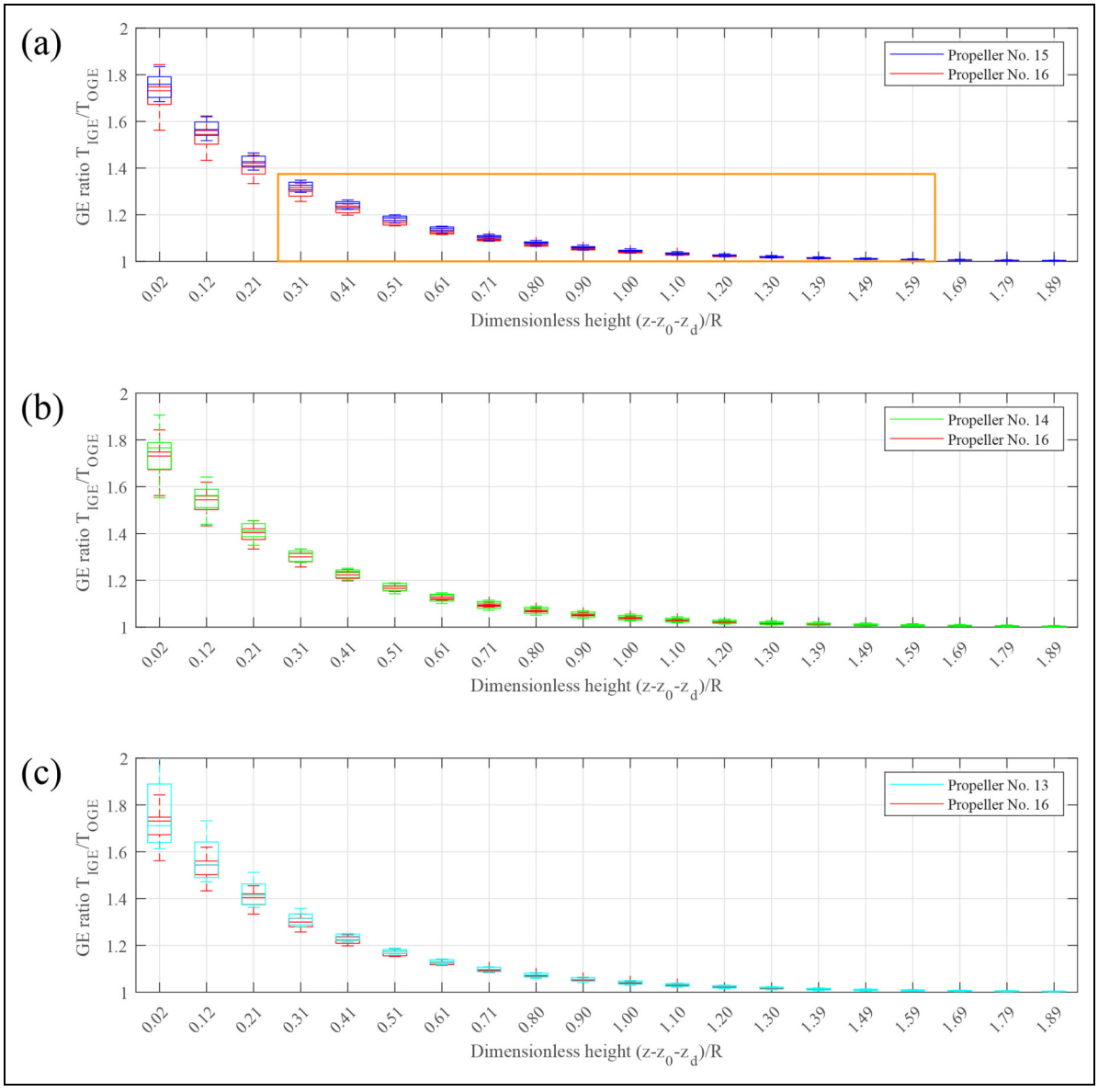

Figure 13. Application of the theory of models comparing propeller 16, as the model, against propellers 15, 14, and 13, as the physical systems, hovering IGE over the surface with adjacent blocks spaced 32-mm apart. (a) Comparison between propellers 16 and 15. Datasets within the orange box indicates the null hypothesis was rejected. (b) Comparison between propellers 16 and 14. (c) Comparison between propellers 16 and 13.

Dimensions from Table 2 show that propeller 15 has a relatively higher pitch angle and 2D-lift curve slope than the others, which contributes to the C_a coefficient. The C_b coefficient, however, is an empirical function of the dimensionless chord length. A further investigation into the governing parameters of C_b could explain the difference.

Since commercially available propellers with fixed dimensions were used, the similarity conditions were more difficult to meet; however, the nondimensional analysis conducted provides justifiable results that support the proposed model.

Connection to partial ground effect

As previously mentioned, the surfaces used in this study have a homogeneous layout. Consider the following, since previous studies have shown that partial ground effect (PGE) is, intuitively, the percentage of the total IGE that interacts with the rotor's wake.[24,27] The principles of PGE for the surfaces in this study may be applied such that at height z the total GE thrust ratio is

$$K_{G,total}(z) = (1 - \lambda_p)K_G(z) + \lambda_p K_G(z + h), \qquad (14)$$

where K_G is the GE thrust ratio over a smooth flat surface and λ_p is the plan area aspect ratio or percentage of the plan area covered by REs of height h. If applied to each surface for each propeller then compared to the average measured data, the average RMSE is 0.007% with the highest being 0.06%. The results show that using PGE is accurate. However, many real world surfaces are not so rigidly homogeneous. This work shows a viable alternative to determine IGE where the factors for PGE are not so easily defined.

Conclusions

This paper first investigated the effects of surface roughness on IGE. Next, a nondimensional IGE model that incorporates the aerodynamic roughness length and zero-plane displacement height was described. Experiments were performed to validate the proposed model's accuracy, where the aerodynamic parameters for artificially-rough surfaces were gathered and the strength of the ground effect over each test surface was measured using multiple COTS propellers of varying sizes. Ground effect test results showed that aerodynamically rougher surfaces corresponded to higher IGE thrust. Statistical analysis of the results confirm the accuracy of the proposed model. The average RMSE found for all experiments was 0.90% and the averaged maximum error was 2.39%, both within the natural noise of the observed GE. Finally, nondimensional analysis confirmed that where similarity conditions are met, the proposed model follows theoretical projections. The work done here has greater implications for more accurate GE compensation over rough surfaces and improvements in UAV motion control, navigation, and design.

Acknowledgments

Authors thank Dr. Xiang He for his time in technical discussions related to the project.

ORCID iD

Kam K Leang https://orcid.org/0000-0003-1189-1673

Funding

The author(s) received no financial support for the research, authorship, and/or publication of this article.

Declaration of conflicting interests

The author(s) declared no potential conflicts of interest with respect to the research, authorship, and/or publication of this article.

References

1. Mahony R, Kumar V and Corke P. Multirotor aerial vehicles: modeling, estimation, and control of quadrotor. *IEEE Robot Autom Maga* 2012; 19: 20–32.
2. Freeman PK and Freeland RS. Agricultural UAVs in the U.S.: potential, policy, and hype. *Remot Sens Appl: Soc Environ* 2015; 2: 35–43.
3. Mohammed F, Idries A, Mohamed N, et al. UAVs for smart cities: opportunities and challenges. In: *International conference on unmanned aircraft systems (ICUAS)*, 2014, pp.267–273.
4. Bhardwaj A, Sam L, Akanksha A, et al. UAVs as remote sensing platform in glaciology: Present applications and future prospects. *Remote Sens Environ* 2016; 175: 196–204.
5. Rosser K, Pavey K, FitzGerald N, et al. Autonomous chemical vapour detection by micro UAV. *Remote Sens (Basel)* 2015; 7: 16865–16882.
6. Bourne JR, Pardyjak ER and Leang KK. Coordinated bayesian-based bioinspired plume source term estimation and source seeking for mobile robots. *IEEE Trans Robot* 2019; 35: 967–986.
7. He X, Bourne J, Steiner J, et al. Autonomous chemical sensing aerial robot for urban/suburban environmental monitoring. *IEEE Syst J* 2019; 13: 3524–3535.
8. Steiner J, Bourne J, He X, et al. Chemical-source localization using a swarm of decentralized unmanned aerial vehicles for urban/suburban environments. In: *ASME dynamic systems and control conference (DSCC), Park City, Utah, October 8-11*, 2019.
9. He X, Bourne J, Steiner J, et al. Gaussian-based kernel for multi-agent aerial chemical-plume mapping. In: *ASME dynamic systems and control conference (DSCC), Park City, Utah, October 8-11*, 2019.
10. Bourne J, Goodell M, He X, et al. Decentralized multi-agent information-theoretic control for target estimation and localization: Finding chemical leaks. *Int J Robot Res* 2020; 39: 1525–1548.
11. Cheeseman I and Bennett W. The effect of the ground on a helicopter rotor in forward flight. ARC Technical Report no. 3021, 1957.
12. Leishman JG. *Principles of Helicopter Aerodynamics*. 2nd ed Cambridge Aerospace Series, Cambridge, MA, USA: Cambridge Univ. Press, 2006. ISBN 9780521858601.
13. Prouty R. Ground effect and the helicopter - a summary. In: *Aircraft design systems and operations meeting*, 1985.
14. Sanchez-Cuevas P, Heredia G and Ollero A. Characterization of the aerodynamic ground effect and its influence in multirotor control. *Int J of Aerosp Eng* 2017; 2017: 1823056.
15. He X and Leang KK. Quasi-steady in-ground-effect model for single and multi-rotor aerial vehicles. *AIAA Journal* 2020; 58: 5318–5331.
16. Eberhart GM. *Modeling of ground effect benefits for multirotor small unmanned aerial systems at hover*. Master's Thesis, Dept. Mech. Eng., Ohio Univ., Athens, OH, 2017.
17. Betz A. The ground effect on lifting propellers. Report Number: NACA-TM-836, Vol. 17, No. 2, April 1937.
18. He X, Kou G, Calaf M, et al. Multi-rotor in-ground-effect modeling and adaptive nonlinear disturbance observer for closed-loop UAV control. *ASME J Dyn Syst Meas and Cont, Special Issue: Autonomous Mobile Systems in Memory of Professor J Karl Hedrick* 2019; 141: 071013.

19. Matus-Vargas A, Rodriguez-Gomez G and Martinez-Carranza J. Ground effect on rotorcraft unmanned aerial vehicles: a review. *Intell Serv Robot* 2021; 14: 99–118.
20. Wierema M. *Design, implementation and flight test of indoor navigation and control system for a quadrotor UAV*. Master's Thesis, Delft University of Technology, 2008.
21. Danjun L, Yan Z, Zongying S, et al. Autonomous landing of quadrotor based on ground effect modelling. In: *2015 34th Chinese control conference (CCC)*, 2015, pp.5647–5652.
22. Sanchez-Cuevas PJ, Heredia G and Ollero A. Multirotor UAS for bridge inspection by contact using the ceiling effect. In: *2017 International conference on unmanned aircraft systems (ICUAS)*, 2017, pp.767–774.
23. Serra P, Cunha R and Silvestre C. On the design of rotorcraft landing controllers. In: *16th Mediterranean conference on control and automation*, 2008, pp.1264–1269.
24. He X. *Modeling and control of in-ground effect of rotorcraft unmanned aerial vehicles*. PhD Thesis, University of Utah, 2020.
25. Fradenburgh EA. The helicopter and the ground effect machine. *J Am Helic Soc* 1960; 5: 24–33.
26. Keshavarzian H and Daneshjou K. Modified under-actuated quadrotor model for forwarding flight in the presence of ground effect. *Aeros Sci Technol* 2019; 89: 242–252.
27. Xin H, Prasad J and Peters D. An analysis of partial ground effect on the aerodynamics of a helicopter rotor. In: *38th Aerospace sciences meeting and exhibit*, 2000, p.262.
28. Cai J, Gunasekaran S and Ol M. Effect of partial ground and partial ceiling on propeller performance. *J Aircr* 2023; 60: 648–661.
29. Kan X, Thomas J, Teng H, et al. Analysis of ground effect for small-scale UAVs in forward flight. *IEEE Robot Autom Lett* 2019; 4: 3860–3867.
30. Curtiss H, Erdman W and Sun M. Ground effect aerodynamics. In: *International conference on. rotorcraft basic research*, 1985.
31. Curtiss H, Sun M, Putman W, et al. Rotor aerodynamics in ground effect at low advance ratios. *J Am Helicop Soc* 1984; 29: 48–55.
32. Bernard DDC, Riccardi F, Giurato M, et al. A dynamic analysis of ground effect for a quadrotor platform. *IFAC-PapersOnLine* 2017; 50: 10311–10316.
33. Hayden JS. The effect of the ground on helicopter hovering power required. In: *Proc. 32nd Annual national V/STOL forum of the american helicopter soc*, 1976.
34. Pulla DP. *A study of helicopter aerodynamics in ground effect*. PhD Thesis, The Ohio State University, 2006.
35. Light JS. Tip vortex geometry of a hovering helicopter rotor in ground effect. *J Am Helicopt Soc* 1993; 38: 34–42.
36. He X. *Modeling and control of in-ground effect on rotorcraft unmanned aerial vehicles*. Thesis, University of Utah, 2020.
37. He X and Leang KK. Quasi-steady in-ground-effect model for single and multi-rotor aerial vehicles. *AIAA J* 2020; 58: 5318–5331.
38. Stuff RB. *An Introduction to Boundary Layer Meteorology*. Dordrecht, The Netherlands: Kluwer Academic Publishers, 1988.
39. Garratt JR. *The atmospheric boundary layer*. Cambridge: Cambridge University Press, 1992.
40. Grimmond C and Oke TR. Aerodynamic properties of urban areas derived from analysis of surface form. *J Appl Meteorol* 1999; 38: 1262–1292.
41. Macdonald RW, Griffiths RF and Hall DJ. An improved method for the estimation of surface roughness of obstacle arrays. *Atmos Environ* 1998; 32: 1857–1864.
42. Holland D, Berglund J, Spruce J, et al. Derivation of effective aerodynamic surface roughness in urban areas from airborne liDAR terrain data. *J Appl Meteorol Climatol* 2008; 47: 2614–2626.
43. Kent CW, Grimmond S and Gatey D. Aerodynamic roughness parameters in cities: inclusion of vegetation. *J Wind Eng Indust Aerod* 2017; 169: 168–176.
44. Lettau H. Note on aerodynamic roughness-parameter estimation on the basis of roughness-element description. *J Appl Meteorol (1962-1982)* 1969; 8: 828–832.
45. Abtew W, Gregory JM and Borrelli J. Wind profile: estimation of displacement height and aerodynamic roughness. *Trans ASAE* 1989; 32: 521–0527.
46. Fang C and Sill B. Aerodynamic roughness length: correlation with roughness elements. *J Wind Eng Indust Aerod* 1992; 41: 449–460.
47. Wierngа J. Representative roughness parameters for homogeneous terrain. *Boundary Layer Meteorol* 1993; 63: 323–363.
48. Counihan J. Wind tunnel determination of the roughness length as a function of the fetch and the roughness density of three-dimensional roughness elements. *Atmosph Environ (1967)* 1971; 5: 637–642.
49. Kutzbach JE. Investigations of the modification of wind profiles by artificially controlled surface roughness. *Stud Three Dimen Struct Planet Bound Layer* 1961; 61.08.K1: 71–113.
50. Nikuradse J. Laws of flow in rough pipes, 1933.
51. Gul M and Ganapathisubramani B. Revisiting rough-wall turbulent boundary layers over sand-grain roughness. *J Fluid Mech* 2021; 911: A26.
52. Perry AE, Schofield WH and Joubert PN. Rough wall turbulent boundary layers. *J Fluid Mech* 1969; 37: 383–413.
53. Munson BR, Young DF, Okiishi TH, et al. *Fundamentals of fluid mechanics, sixth edition*. Hoboken: Don Fowley, 1990.
54. Cai J, Gunasekaran S, Ahmed A, et al. Propeller partial ground effect. In: *AIAA Scitech 2020 Forum*, 2020, pp.1028.
55. Cai J and Gunasekaran S. Propeller ground effect in forward flight. *AIAA J Am Inst Aeronaut Astron* 2023; 61: 4378–4390.
56. Cai J, Gunasekaran S, Ahmed A, et al. Changes in propeller performance due to ground proximity. In: *AIAA scitech 2019 forum*, 2019, pp.1097.
57. Hansen FV. Surface roughness lengths. Technical report, Army Research Lab White Sands Missile Range, NM, 1993.
58. Bradford G. *Investigations of surface roughness length modification in black rock City, Nevada*. Master's Thesis, San Francisco State University, 2015.

59. Sullivan R and Greeley R. *Aerodynamic roughness measured in the field and simulated in a wind tunnel*, NASA Technical Report, Report no. NASA-CR-4422, 1992.
60. Counihan J. An improved method of simulating an atmospheric boundary layer in a wind tunnel. *Atmosph Environ (1967)* 1969; 3: 197–214.
61. Kozmar H. Characteristics of natural wind simulations in the tum boundary layer wind tunnel. *Theor Appl Climatol* 2011; 106: 95–104.
62. Bernard DDC, Giurato M, Riccardi F, et al. Ground effect analysis for a quadrotor platform. In: *Advances in aerospace guidance, navigation and control*, 2018. pp.351–367. Springer.
63. Student The probable error of a mean. *Biometrika* JSTOR, 1908, pp.1–25.
64. Wasserstein RL and Lazar NA. The ASA statement on p-values: context, process, and purpose. *Am Stat Taylor Francis* 2016; 70: 129–133.